Article

Not peer-reviewed version

Magnetic Field Suppression of the Martensitic Transformation in Mn-Based MnNi(Fe)Sn Metamagnetic Shape Memory Heusler Alloys

Patricia Lázpita *, Natalia Ahiova Río-López, David Mérida, Emily Leonie Quinlyn Nowalaja Ammerlaan, Uli Zeitler, Volodymyr Chernenko, Jon Gutiérrez *

Posted Date: 17 July 2025

doi: 10.20944/preprints202507.1421.v1

Keywords: Heusler metamagnetic shape memory alloy; martensitic transformation; kinetic arrest; magnetic field phase diagram

 doi:10.20944/preprints202507.1421.v1

Article

Magnetic Field Suppression of the Martensitic Transformation in Mn-Based MnNi(Fe)Sn Metamagnetic Shape Memory Heusler Alloys

Patricia Lázpita [1,2,*], Natalia Ahiova Río-López [1,2], David Mérida [1], Emily (Leonie Quinlyn Nowalaja) Ammerlaan [3], Uli Zeitler [3], Volodymyr Chernenko [1,2] and Jon Gutiérrez [1,2,*]

[1] University of the Basque Country UPV/EHU, Barrio Sarriena s/n, 48940 Leioa, Spain; nataliaahiova.rio@ehu.eus (N.A.R.-L.); david.merida@ehu.eus (D.M.); volodymyr.chernenko@ehu.eus (V.C.)

[2] BCMaterials, Martina Casiano Building, UPV/EHU Scientific Park, Barrio Sarriena s/n, 48940 Leioa, Spain

[3] High Field Magnet Laboratory (HFML-EMFL), Radboud University, Nijmegen 6525 ED, The Netherlands; nowa.ammerlaan@ru.nl (E.L.Q.N.A.); uli.zeitler@ru.nl (U.Z.)

* Correspondence: patricia.lazpita@ehu.eus (P.L.); jon.gutierrez@ehu.eus (J.G.)

Abstract

Heusler metamagnetic shape memory alloys (MMSMAs) show a large functional response associated with a first order martensitic transformation (MT). The strong magneto-structural coupling together with mixed magnetic interactions enable controlling this MT by means of magnetic field resulting in different multifunctional properties such as giant magnetoresistance, metamagnetic shape-memory effect (MMSM), or inverse magnetocaloric effect (MCE). Both the shift rate of MT as a function of the magnetic field and its eventual suppression are key parameters for the development of all these effects. In this work we present our findings regarding the use of strong steady magnetic fields, up to 33 T, to study in detail the magnetic field induced MT and its suppression in MnNi(Fe)Sn MMSMAs, leading to creation of the T-$\mu_0 H$ phase diagrams of the MT. Moreover, we have analyzed the impact of Fe - doping and, as direct consequence, the magnetic coupling on the suppression of the magnetostructural transformation.

Keywords: Heusler metamagnetic shape memory alloy; martensitic transformation; kinetic arrest; magnetic field phase diagram

1. Introduction

Heusler metamagnetic shape memory alloys (MMSMAs) of the Ni-Mn-X (X=In, Sn, Sb)-type exhibit good physical properties and a remarkable functional response associated with a first order martensitic transformation (MT) [1,2]. The combination of magneto-volume coupling and ferromagnetic-antiferromagnetic interactions in these compounds allows for control of this MT by using an external magnetic field through the effect of magnetic field-induced martensitic transformation (MFIMT). This leads to multifunctional properties, such as the magnetocaloric [3,4] magnetoresistance, magnetostrain and metamagnetic shape memory [5,6] effects, paving so the way for technical applications.

When controlled by a magnetic field, this metamagnetic transformation is directly related to the change in magnetization between the austenitic and martensitic phases at the MT. The well-known Clausius Clapeyron relationship:

$$-\frac{dT_M}{d(\mu_0 H)} = \frac{\Delta M}{\Delta S} \quad (1)$$

(where $\mu_0 H$ is the applied magnetic field, T_M is the MT temperature, and ΔM and ΔS are the magnetization and entropy changes at the MT, respectively) provides insights into the advantages of

 doi:10.20944/preprints202507.1421.v1

searching for alloys that exhibit large ΔM and high magnetostructural coupling, resulting in a large $dT_M/d\mu_0 H$ values, thereby facilitating the magnetic field induced transformation and maintaining a substantial ΔS. To tailor ΔM and T_M, one can modify the composition of the alloy or properly dope it with other elements.

The magnetization in Heusler-like alloys mainly depends on the magnetic moment of Mn atoms and the distance between these atoms, which determine the observed magnetic exchange interactions [7,8]. Clearly, increasing Mn content is a suitable strategy to enhance the ΔM change value, as reported by Xuang *et al.* [9]. The Mn-Mn magnetic interactions can be also altered by doping with another magnetic element, such as the *3d* Fe or Co atoms. For example, in the case of $Mn_{50}Ni_{40}In_{10}$ alloys, doping with a 3 at.% Co increases magnetization from 40 Am^2kg^{-1} to 89 Am^2kg^{-1}, as reported by Wu *et al.* [10]. Lázpita *et al.* [11] reported an increase in ΔM from 19 Am^2kg^{-1} (x=0) to 49 Am^2kg^{-1} (x=4) in $Mn_{49}Ni_{42-x}Fe_xSn_9$ alloys. This doping with additional magnetic atoms also promotes the formation of new secondary phases in the alloy which can be advantageous for enhancing their mechanical characteristics by reducing, for instance, the inherent fragility of these MMSMAs. Moreover, for certain critical concentrations of these dopants, there are changes in the magnetic coupling that can hinder the entire magnetostructural transformation, preventing its progression [12,13]. In these situations, a fascinating phenomenon occurs in MMSMAs, known as the kinetic arrest of MT, which hinders the magnetostructural transition under a sufficiently strong magnetic field [14–16].

The effect of kinetic arrest is related to the total entropy change across the MT, ΔS_T, which must be negative for the direct MT. The total entropy of the MT is expressed as: $\Delta S_T = \Delta S_{lattice} + \Delta S_{magnetic}$, where $\Delta S_{lattice}$ and $\Delta S_{magnetic}$ is the lattice and magnetic entropy, respectively (the electronic entropy contribution can be neglected in these case). In the MMSMAs, the lattice entropy is negative in the direct MT, while the magnetic entropy is positive and lower, due to the transition from a ferromagnetic to a paramagnetic phase, resulting in $\Delta S_T < 0$. In the presence of a magnetic field, $\Delta S_{lattice}$ remains invariant, while $\Delta S_{magnetic}$ increases, the lattice contribution to the total entropy remains constant, while the magnetic contribution increases, eventually leading to a zero total entropy $\Delta S_T \sim 0$, inhibiting or kinetically arresting MT at a critical magnetic field.

There are two methods to investigate the kinetic arrest phenomenon through the study of magnetic properties. The first method is to measure the magnetization (M) as a function of temperature, at different constant magnetic fields (H). The second method is to measure M as a function of H, at various constant temperatures. Thus, MFIMT and related phenomena can be studied by performing Zero Field Cooling (ZFC) measurements starting from the martensitic phase, or by performing Field Cooling (FC) measurements starting either from the martensitic or austenitic phases of the alloy [17]. In this last case the applied field during the FC process can be high enough to arrest the MT. Landazábal *et al.* [18] argued that this arrest may originate from the fact that "the microstructure obtained after ZFC is stable, but the one obtained after FC is in a non-equilibrium state".

In this study we report the outcomes of the impact of high magnetic fields on a series of $Mn_{49}Ni_{42-x}Fe_xSn_9$ ($0<x<6$) of alloys. In particular, for the alloy with x=5 alloy we observed both MFIMT and kinetic arrest at approximately 18 T. However, for the alloy with x = 4, we only observed MFIMT, and no kinetic arrest was detected even at magnetic fields up to 33 T. Such behaviors will be explained in terms of lattice and magnetic entropy contributions.

2. Materials and Methods

Polycrystalline ingots of $Mn_{49}Ni_{42-x}Fe_xSn_9$ with x=0, 2, 3, 4, 5 and 6 were prepared by induction melting of starting high purity metals (>99.9%) and homogenized by heat treatment for 3 days at 1173 K in argon atmosphere. From these ingots small pieces were cut, heat treated during 0.5 h at 1173 K with subsequent quenching in ice water, and finally mechanically polished.

Samples microstructure was examined by scanning electron microscopy (SEM) in a Hitachi TM300 table-top equipped with energy dispersive X-ray (EDX) analysis. This EDX allows to determine compositions values with an uncertainty of about 1 at.%. Room temperature X-ray diffraction patterns were recorded in a Bruker D8 Advance diffractometer by using Cu Kα radiation.

 doi:10.20944/preprints202507.1421.v1

MT temperatures were determined through differential scanning calorimetry curves (DSC Mettler Toledo 822e) measured at heating/cooling rate of 5 K/min. Thermomagnetic and magnetization loops measurements were performed in a vibrating sample magnetometer (VSM, Cryogenic Ltd.) in a range of temperatures from 10 to 320 K, with applied magnetic fields up to 12 T. A home-made VSM was used to carry out measurements at higher temperatures, from 300 K to 450 K and H fields up to 1.8 T. The results of these measurements were published in the reference [11].

In order to establish the T-$\mu_0 H$ phase diagrams for the alloys with x=4 and 5, we carefully determined the influence of the applied magnetic field on the MT by measuring the thermomagnetic curves. The high temperature part of this diagram was obtained by using a vibrating sample magnetometer (Magnetic platform from Cryogenic Ltd. CFMS) in the range of 5-320 K at constant applied fields up to 12 T. To determine the value of the MT temperature for each applied field we used a conventional two-tangent method. The low temperature part of the phase diagram was determined through isothermal magnetization curves, $M(H)$, measured at constant temperatures from 250 K down to 4.2 K under applied fields up to 33 T at the High Field Magnet Laboratory (HFML-EMFL, Radboud University, Nijmegen, The Netherlands). At these low temperatures, it is necessary such a strong magnetic field to ensure the largest possible completeness of the reverse and forward MFIMT.

3. Results and Discussion

3.1. Crystal Structure and Microstructure

Extensive information about this initial characterization method can be found in [11]. Briefly, room temperature X-ray diffraction patterns has revealed three different crystal structures in the bulk samples as the Fe content in their composition increases: the x=0 alloy shows a unique martensite phase with orthorhombic structure. The Fe containing alloys corresponding to x=2, 5 and 6 compositions exhibit the B2 cubic phase with some fcc γ-phase precipitates arising from the Fe addition. Finally, x=3 and 4 alloys show a mixture of three phases: austenite, martensite and fcc γ-phase. It has to be noticed that cell parameters for austenite B2 phase and γ-phase remain practically constant for all Fe containing alloys, a behavior that clearly differs from that observed in NiMnSn alloys doped with Fe [19], with a clear increment of the cubic cell parameter.

SEM images analysis of representative alloys x=0, 4 and 5 show different features. The x=0 alloy exhibits a uniform and unique martensite microstructure. The x=4 and 5 alloys show two different zones: a continuous, light area corresponding to the matrix and a dark area corresponding to random γ-phase precipitates. From EDX analysis we have determined also a fairly good agreement between the measured averaged compositions and the expected nominal ones. On the other hand, the fcc γ-phase percentage in the alloys clearly increases as the Fe content increases, with vol.% percentages that increase from a 1.1 for the x=2 to a 30 % for the x=6 Fe alloys.

3.2. Magnetic Field Influence on the Martensitic Transformation and Kinetic Arrest

To magnetically characterize the MT exhibited by these alloys, thermo-magnetization measurements, $M(T)$, at low magnetic field of 5 mT were performed. These curves are convenient to adequately determine MT temperatures during cooling $T_M=(M_s+M_f)/2$ (where M_s and M_f are the forward MT temperatures, start and finish, respectively), and heating $T_A=(A_s+A_f)/2$ (where A_s and A_f are the reverse MT temperatures, start and finish, respectively) processes, as well as the magnetization change ΔM between the start and the end of the MT, $\Delta M=M^A-M^M$, were M^A and M^M denote magnetization values of the austenite and martensite phases, respectively. Thus, the measured forward MT temperatures linearly decrease from 318 K for the x=0 composition to 223 K for the x=4 sample, with a slope of -22 K/at.%Fe. In clear contrast, the x=5 and x=6 Fe content compositions show an almost constant transformation temperature of about 80 K. With regard to the magnetization change (ΔM), it was evaluated through thermomagnetic measurements at a magnetic field of 9 T in order to analyze the maximum magnetization difference between the martensite and austenite phases. The ΔM value increases from the x=0 to the x=4 alloys (from 18 to 50 Am^2kg^{-1}, respectively), and suffers a sharp drop

 doi:10.20944/preprints202507.1421.v1

to 8 Am^2kg^{-1} for x=5, and almost vanishes for the x=6 composition. Figures 4 and 5 in Reference [11] properly describe this previous MT magnetic characterization.

The significant difference observed between the x=4 and x=5 composition alloys in terms of thermo-magnetic measurements fully justifies the need for a more in-depth study of their magnetization transformation behavior, in particular an extensive analysis of the effect of the magnetic field on the MT under different routes as ZFC and FC conditions.

Figure 1 shows recorded thermo-magnetic curves for the x=4 (measured up to 12 T) and x=5 (measured up to 9 T). The lowest applied magnetic field intensity measured curve allows for the determination of the Curie temperature of the alloy as the minimum of the *dM/dT* dependence. Thus, austenite Curie temperatures about 296 K for the x=4 alloy and 283 K for the x=5 alloy were determined.

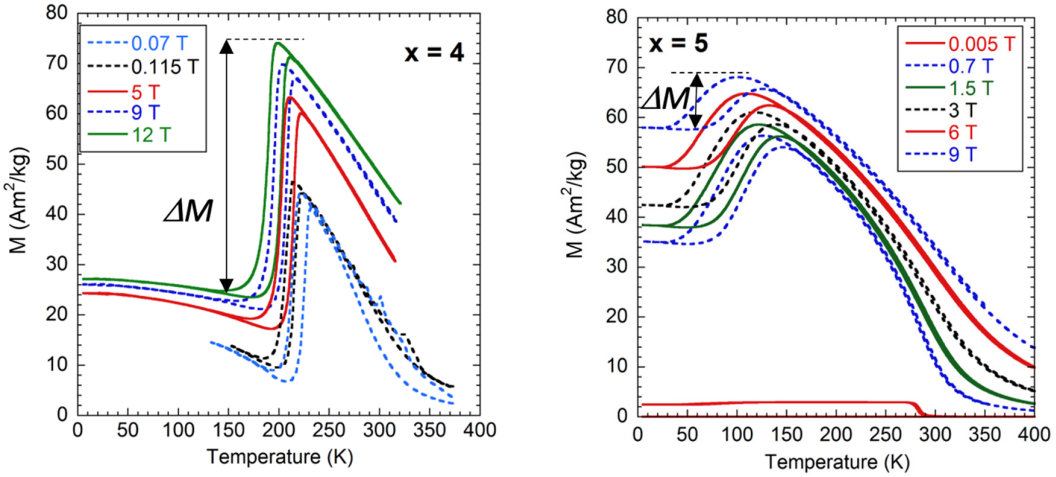

(**a**) (**b**)

Figure 1. Thermo-magnetization curves measured for $Mn_{49}Ni_{42-x}Fe_xSn_9$ alloys with: (**a**) x= 4 composition; (**b**) x=5 composition.

It is evident that the applied magnetic field has a significant influence on both the MT temperature and the observed ΔM value. As the applied magnetic field increases, the MT temperatures decrease away from the Curie temperature. This behavior promotes the enhancement of magnetization in both the austenite and martensite phases. However, the evolution of ΔM differs notably between the two alloys. In the x=4 alloy, the magnetic field favors the MT, with ΔM values increasing from 35 to 50 Am^2kg^{-1} as the applied magnetic field increases from 0 to 12 T. That is, the field-induced magnetization increment in the austenite phase is greater than that in the martensite phase. In contrast, the x=5 alloy exhibits a decrease in ΔM from 20 to 10 Am^2kg^{-1} as the magnetic field increases from 0 to 9 T. This alloy experiences a significant ΔM increase at low applied fields (up to 0.7 T), followed by a decrease at higher magnetic fields, indicating that the magnetic field H can inhibit the MT.

To further analyze this observed behavior, we measured isothermal magnetization curves $M(H)$ under ZFC conditions above and below the corresponding MT temperatures for both alloys. Figure 2a shows such measurements for the x=4 Fe content alloy (T_M = 223 K). The curve recorded at 230 K is clearly in the ferromagnetic austenite phase. Curves measured at 200 and 174 K, temperatures where only the martensite structure is expected to appear within this alloy, show an increase in the magnetization value when the magnetic field is applied indicating MFIMT which starts at the austenitic start magnetic field (H_{AS}) with a reversible metamagnetic effect. The measured behavior goes from the low magnetization value of the weak-magnetic martensite to the high magnetization one of the ferromagnetic austenite. The measurement performed at 151 K, shows the remaining martensite magnetization, as expected much lower that the austenite one. At this temperature a full MFIMT is not observed for magnetic fields up to 33 T, displaying only a small increment in the magnetization trend related to a partial MT. Figure 2b shows graphically measured magnetization values determined in FC

 doi:10.20944/preprints202507.1421.v1

conditions where the MT takes place completely under 30 T of the applied magnetic field, i.e., there is no arrested austenite and the kinetic arrest effect does not occur. The inset clearly indicates that at low temperature (142 K in Figure 2b) the alloy presents a weakly magnetic martensite which is not affected by the cooling conditions, showing the same behavior for ZFC and FC protocols.

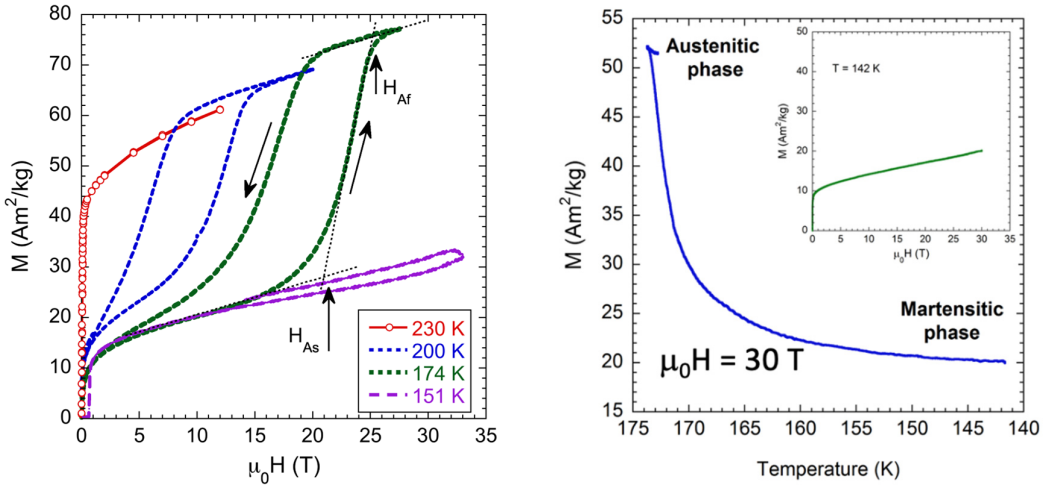

Figure 2. (**a**) ZFC magnetization loops (at the first quadrant) at different temperatures and a maximum applied H field of 33 T measured for the x=4 Fe content alloy; (**b**) Measured magnetization evolution as a function of temperature at an applied H field of 30 T. The inset shows the magnetic field induced magnetization of the martensite, measured at 142 K after 30 T FC condition.

The measured isothermal magnetization curves *M(H)* together with the isomagnetic field magnetization ones *M(T)* allow also for the construction of a $T - \mu_0 H$ phase diagram of the characteristic temperatures of the MT. This is shown in Figure 3.

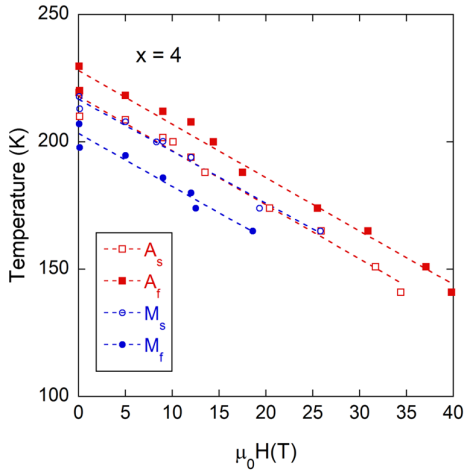

Figure 3. $T - \mu_0 H$ phase diagram of the characteristic temperatures of the MT for the $Mn_{49}Ni_{38}Fe_4Sn_9$ alloy (x=4).

As observed, there is a quasi-linear dependence of all determined $A_{s,f}$ and $M_{s,f}$ temperature values, with a negative slope of about -2.25 K/T, practically equal for all these transformation temperatures. Besides, kinetic arrest of the MT has not been reached for applied magnetic fields as high as ~30 T. The lack of data for M_{fs} at high applied magnetic fields is just due to experimental set-up limitations.

Figure 4a shows similar measurements performed for the x=5 Fe alloy (T_M = 80 K). The curve recorded at 100 K is in the austenite phase and shows mostly a ferromagnetic behavior. The loop

 doi:10.20944/preprints202507.1421.v1

measured at 62 K (practically at the end of the MT) and 30 K (at the martensite phase) are quite similar in shape, and clearly the martensitic phase contribution to magnetization at low magnetic field and a partial reversible MFIMT which starts at H_{AS} = 7 T and 11 T is observed. Finally, curve measured at 4 K presents a similar behavior but its width increases, indicating that the reversibility of the MFIMT is restricted and that the fraction of the non-transformed martensite increases, due to the magnetic field austenite phase arrest. Moreover, the austenitic phase obtained across the MFIMT is stable over a larger field range as the temperature decreases. Also, measured magnetization value at the highest applied field of 33 T, at those previous temperatures, slightly increase, indicating that a higher percentage of austenite phase is induced, although it can also be explained by increased saturation magnetization at low temperatures. Figure 4b shows the measured *M(H)* behavior at 4 K when this temperature is reached in ZFC and FC conditions. While the shape of the two loops is quite similar, it turns out to be lower the martensitic saturation magnetization when it is measured after ZFC conditions. This fact clearly indicates that the FC protocol partially retains the MT, with the presence of a ferromagnetic austenite phase that reflects in the increase of the saturation magnetization at low magnetic field. Moreover, at this low temperature the applied magnetic field is still able to induce some transformation of the martensite. The H_{AS} is higher for the FC protocol due to the lower fraction of martensitic phase that can transform in this case.

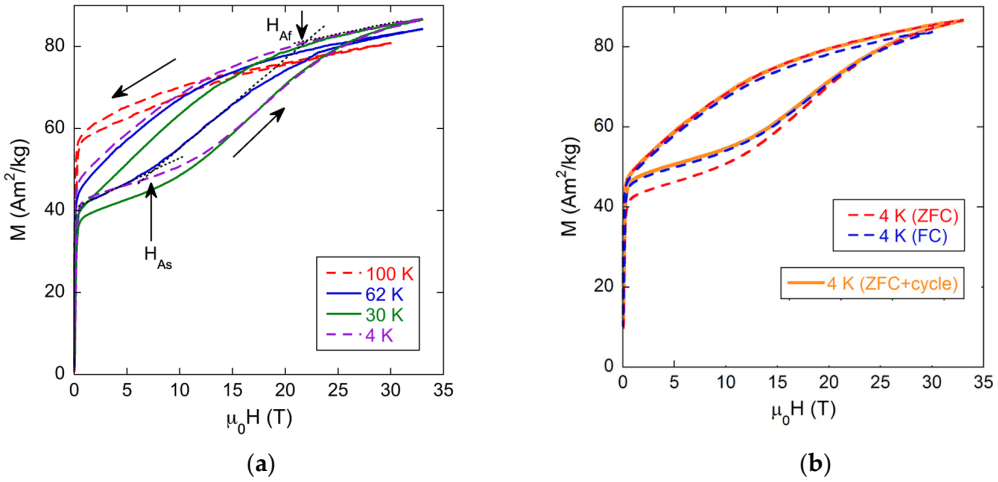

Figure 4. (**a**) Magnetization loops (at the first quadrant) measured at different temperatures for the x=5 Fe content alloy; (**b**) Magnetization loops (at the first quadrant) at 4 K and measured under ZFC and FC conditions. In both cases a maximum applied H field of 33 T has been used.

Again, from measured isothermal magnetization curves *M(H)*, the $T - \mu_0 H$ phase diagram of the characteristic temperatures of the MT can be constructed. This is shown in Figure 5. The behavior of MT temperatures is now drastically different from the previously shown for the x=4 alloy. At temperatures above 50 K, transformation characteristic temperatures decrease in a strong non-linear manner as the applied magnetic field increases. Nevertheless, at temperatures lower than 50 K two behaviors can be observed: on the one hand, applied magnetic fields required to induce the reverse MT are practically constants up to 4 K and do not change with decreasing temperature (H_{As} about 11 T and H_{Af} about 25 T). On the other hand, applied magnetic fields required to induce the direct MT are lower when temperatures drop, reaching a minimum of 14 T at 4 K. In fact, at the lowest temperatures, there is a remarkable split between the M_s and A_f temperatures evolution curves. This observation arises from the fact that ZFC or FC processes below 50 K have a different impact in the state (either stable or non-equilibrium, depending on the cooling process) of the martensite phase of the x=5 sample. The lack of data for M_f at lowest temperatures is related to the fact that the direct MT is partially inhibited when it occurs after the application of a magnetic field. Then, Figure 5 represents

 doi:10.20944/preprints202507.1421.v1

what is already known in MMSMAs as the kinetic arrest effect [14–16] in which the austenite phase is, for this x=5 alloy, “frozen” or "blocked" for applied magnetic fields higher than ~17 T.

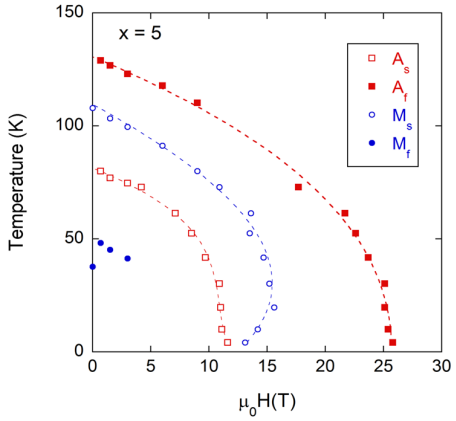

Figure 5. Transformation temperatures versus magnetic field diagram for the $Mn_{49}Ni_{37}Fe_5Sn_9$ alloy.

Based on our observations, we can explain the distinct behavior of our $Mn_{49}Ni_{42-x}Fe_xSn_9$ alloys with x=4 and x=5 by considering the influence of the Fe content on the magnetic and martensitic transition (MT) characteristics of these two compositions. Neither of these alloys exhibits magnetic saturation for applied magnetic fields up to 33 T, which clearly indicates the presence of antiferromagnetic (AFM) coupling when Ni atoms are substituted by Fe. A slight change in the Fe content, from x=4 to x=5, leads to a drastic alteration in the magnetization change, ΔM, of each alloy. Evaluating the ZFC isothermal magnetization curves, the x=4 alloy exhibits a maximum ΔM value of about 50 Am^2kg^{-1} at 174 K, while the x=5 alloy shows just a maximum ΔM value of 30 Am^2kg^{-1} at 30 K, moreover, both values remain almost constant when the martensitic transformation is fully developed. This variation represents a 40% reduction of the magnetization change when the Fe doping increases in a 1%. If we assume that the austenitic phase saturation magnetization is similar in both alloys (around 80 Am^2kg^{-1}) the ΔM decrease can be related to the increase of the magnetization of the martensitic phase indicating that the Fe doping favors the ferromagnetic coupling over antiferromagnetic one of the martensitic phase. This change in magnetic coupling would directly impact the magnetic entropy variation in the transformation $\Delta S_{magnetic}$, allowing the arrested kinetic process for the higher Fe alloy.

Analyzing the observed behavior in terms of entropy change which is considered as arising from lattice vibrational and magnetic contributions, $\Delta S = \Delta S_{lattice} - \Delta S_{magnetic}$, and assuming that $\Delta S_{lattice}$ is not influenced by the applied magnetic field, it is clear that the cooling process of the alloys during measurements as well as the presence of retained austenite at very low temperatures influence directly the $\Delta S_{magnetic}$ magnitude. In the case of $|\Delta S_{lattice}| = |\Delta S_{magnetic}|$, $\Delta S \sim 0$ and the kinetic arrest occurs. This is the situation shown in Figure 5 for the x=5 alloy. Most probably, this kinetic arrest is also enhanced by the present amount of γ-phase inside this alloy: while for the x=4 alloy composition a vol.% of 13.3 has been determined, this percentage increases up to a 19.1 for the x=5 alloy [11]. Precipitates increase the internal stresses which could favor the appearance of the kinetic arrest in the latter alloy.

4. Conclusions

The Fe doping of Mn-Ni-Sn metamagnetic alloys opens up the possibility to study a wide range of the magnetic field induced phenomena, such as changes in magnetization (ΔM), changes in the MT temperatures (T_M) and the associated transformation entropy (ΔS), and even the occurrence of the kinetic arrest process. Slight changes in the composition of $Mn_{49}Ni_{42-x}Fe_xSn_9$ alloys from x=4 to 5 result in completely different behaviors. The alloy with x=4 shows large ΔM = 50 Am^2kg^{-1} at 174 K and MT temperatures $A_{s,f}$ and $M_{s,f}$ with a negative slope of about -2.25 K/T for applied magnetic fields up to 40 T, and there is no trace of kinetic arrest of MT at these high applied fields . In contrast, the x=5

 doi:10.20944/preprints202507.1421.v1

alloy exhibits a significantly reduced ΔM = 30 Am^2kg^{-1} at 30 K. The MT temperatures evolve in a strongly non-linear manner as the temperature decreases and the applied magnetic field increases. For applied magnetic fields greater than ~17 T, the MT kinetic arrest occurs. The origin of this kinetic arrest can be attributed to the amount of retained austenite in the $Mn_{49}Ni_{37}Fe_5Sn_9$ alloy. This is likely favored not only by the cooling process under magnetic field during the measurements, but also by the presence of the fcc γ-phase in the alloy.

Author Contributions: Conceptualization, P.L., V.C. and J.G.; methodology, P.L., N.A.R.-L., D.M. and V.C.; validation, N.A.R.-L., D.M., A.A. and U.Z.; investigation, N.A.R.-L., D.M., A.A. and U.Z.; writing—original draft preparation, P.L. and J.G.; supervision, J.G.; project administration, J.G. and P.L. All authors discussed the results and contributed to the final manuscript. All authors have read and agreed to the published version of the manuscript.

Funding: This research was funded by the Grant PID2022-138108OB-C33 funded by MICIU/AEI/10.13039/501100011033, Project IT1479-22

Institutional Review Board Statement: Not applicable.

Informed Consent Statement: Not applicable.

Data Availability Statement: The data are contained within the article.

Acknowledgments: P.L., N.A.R.-L., D.M. and J.G. gratefully acknowledge the Spanish Ministerio de Ciencia, Innovación y Universidades for financial support under Grant PID2022-138108OB-C33 funded by MICIU/AEI/10.13039/501100011033 and by the European Union Next Generation EU/PRTR. the financial support of the Basque Government under Research Groups Programme IT1479-22 projects and research project IKUR_IKA_25/03 (Ikerbasque Foundation, Basque Foundation for Science, Basque Government). Technical and human support provided by the General Research Services of the UPV/EHU (SGIker) is gratefully acknowledged.

Conflicts of Interest: The authors declare no conflicts of interest.

Abbreviations

The following abbreviations are used in this manuscript:

MMSMA	Heusler metamagnetic shape memory alloy
MT	Martensitic transformation
MMSM	Metamagnetic shape memory effect
MCE	Magnetocaloric effect
MFIMT	Magnetic field induced transformation
ZFC	Zero Field Cooling
H/SFC	High/Super Field Cooling
DSC	Differential Scanning Calorimetry
VSM	Vibrating Sample Magnetometry/Magnetometer

References

1. Kainuma R.; Imano Y.; Ito W; Sutou Y.; Morito H.; Okamoto S.; Kitakami O.; Oikawa K.; Fujita A.; Kanomata T.; Ishida K. Magnetic-field-induced shape recovery by reverse phase transformation. *Nature* **2006**, 439, 957-960; https://doi.org/10.1038/nature04493.
2. Yu S.Y.; Cao Z.X.; Ma L.; Liu G.D.; Chen J.L.; Wu G.H.; Zhang B.; Zhang X.X. Realization of magnetic field-induced reversible martensitic transformation in NiCoMnGa alloys. *Appl. Phys. Lett.* **2007**, 91, 102507; https://doi.org/10.1063/ 1.2783188.
3. Krenke T.; Duman E.; Acet M.; Wassermann E.F.; Moya X.; Mañosa L.; Planes A. Inverse magnetocaloric effect in ferromagnetic Ni-Mn-Sn alloys. *Nat. Mater.* **2005**, 4, 450-454; https://doi.org/10.1038/nmat1395.

 doi:10.20944/preprints202507.1421.v1

4. Castillo-Villa P.O.; Mañosa L.; Planes A.; Soto-Parra D.E.; Sánchez-Llamazares J.L.; Flores-Zúñiga H.; Frontera C. Elastocaloric and magnetocaloric effects in Ni-Mn-Sn(Cu) shape-memory alloy. *J. Appl. Phys.* **2013**, 53506, 1-6; https://doi.org/10.1063/1.4790140.
5. Kainuma R.; Oikawa K.; Ito W.; Sutou Y.; Kanomata T.; Ishida K. Metamagnetic shape memory effect in NiMn-based Heusler-type alloys. *J. Mater. Chem.* **2008**, 18, 1837; https://doi.org/10.1039/b713947k.
6. Ito K.; Ito W.; Umetsu R.Y.; Tajima S.; Kawaura H.; Kainuma R.; Ishida K. Metamagnetic shape memory effect in polycrystalline NiCoMnSn alloy fabricated by spark plasma sintering. Scripta Mater. 2009, 61, 504-507; https://doi.org/10.1016/j.scriptamat.2009.05.008.
7. Enkovaara J.; Heczko O.; Ayuela A.; Nieminen R.M. Coexistence of ferromagnetic and antiferromagnetic order in Mn-doped Ni_2MnGa. *Phys. Rev. B* **2003**, 63, 212405; https://doi.org/10.1103/PhysRevB.67.212405.
8. Richard M.L.; Feuchtwanger J.; Allen S.M.; O'Handley R.C.; Lazpita P.; Barandiarán J.M.; Gutiérrez J.; Ouladdiaf B.; Mondelli C.; Lograsso T.A.; Schlagel D.L. Chemical order in off-stoichiometric Ni-Mn-Ga ferromagnetic shape-memory alloys studied with neutron diffraction. *Philos. Mag. A* **2007**, 87, 3437-3447; https://doi.org/10.1080/14786430701297582.
9. Xuang H.C.; Ma S.C.; Cao Q.Q.; Wang D.H.; Du Y.W. Martensitic transformation and magnetic properties in high-Mn content $Mn_{50}Ni_{50-x}In_x$ ferromagnetic shape memory alloys. *J. Alloy Comp.* **2011**, 509, 5761-5764; https://doi.org/10.1016/j.jallcom.2011.01.073.
10. Wu Z.; Liu Z.; Yang H.; Liu Y.; Wu G. Metamagnetic phase transformation in $Mn_{50}Ni_{37}In_{10}Co_3$ polycrystalline alloy. *Appl. Phys. Lett.* **2011**, 98, 61904; https://doi.org/10.1063/1.3554423.
11. Lázpita P.; Sasmaz M.; Barandiarán J.M.; Chernenko V.A. Effect of Fe doping and magnetic field on martensitic transformation of Mn-Ni(Fe)-Sn metamagnetic shape memory alloys. *Acta Materialia* **2018**, 155, 95-103; https://doi.org/10.1016/j.actamat.2018.05.052.
12. Wu Z.; Liu Z.; Yang H.; Liu Y.; Wu G.; Woodward R.C. Metallurgical origin of the effect of Fe doping on the martensitic and magnetic transformation behaviours of $Ni_{50}Mn_{40-x}Sn_{10}Fe_x$ magnetic shape memory alloys. *Intermetallics* **2011**, 19, 445-452; https://doi.org/10.1016/j.intermet.2010.10.010.
13. Tan C.; Tai Z.; Zhang K.; Tian X.; Cai W. Simultaneous enhancement of magnetic and mechanical properties in Ni-Mn-Sn alloy by Fe doping, *Sci. Rep.* **2017**, 7, 2-10; https://doi.org/10.1038/srep43387.
14. Ito W.; Ito K.; Umetsu R.Y.; Kainuma R.; Koyama K.; Watanabe K.; Fujita A.; Oikawa K.; Ishida K.; Kanomata T. Kinetic arrest of martensitic transformation in the NiCoMnIn metamagnetic shape memory alloy. *Appl. Phys. Lett.* **2008**, 92, 021908; https://doi.org/10.1063/1.2833699.
15. Xu X.; Ito W.; Tokunaga M.; Umetsu R.Y.; Kainuma R.; Ishida K. Kinetic arrest of martensitic transformation in NiCoMnAl metamagnetic shape memory alloy. *Mater. Trans.* **2010**, 51, 1357-1360; https://doi.org/10.2320/matertrans.M2010098.
16. Umetsu R.Y.; Xu X.; Ito W.; Kihara T.; Takahashi K.; Tokunaga M.; Kainuma R. Magnetic field-induced reverse martensitic transformation and thermal transformation arrest phenomenon of $Ni_{41}Co_9Mn_{39}Sb_{11}$ alloy. *Metals* **2014**, 4, 609–622; https://doi.org/10.3390/met4040609.
17. Lázpita P.; Pérez-Checa A..; Barandiarán J.M.; Ammerlan A.; Zeitler U.; Chernenko V.A. Suppression of martensitic transformation in Ni-Mn-In metamagnetic shape memory alloy under very strong magnetic field. *Journal of alloys and Compounds* **2021**, 874, 159814 (6 pp.); doi: 10.1016/j.jallcom.2021.159814.
18. Pérez-Landazábal J.I.; Recarte V.; Sánchez-Alarcos V.; Gómez-Polo C.; Kustov S.; Cesari E. Magnetic field induced martensitic transformation linked to the arrested austenite in a Ni-Mn-In-Co shape memory alloy. *J. Appl. Phys.* **2011**, 109, 093515; https://doi.org/10.1063/1.3585827.
19. Aguilar-Ortiz C.O.; Soto-Parra D.E.; Alvarez-Alonso P.; Lázpita P.; Salazar D.; Castillo-Villa P.O.; Flores-Zúñiga H.; Chernenko V.A. Influence of Fe doping and magnetic field on martensitic transition in Ni-Mn-Sn melt-spun ribbons. *Acta Mater.* **2016**, 107, 9-16; https://doi.org/10.1016/j.actamat.2016.01.041.